

Resonant frequencies of circular-sided dual-port microstrip antenna

S.O. Kundukulam, M. Paulson, C.K. Aanandan, P. Mohanan and K.G. Nair

Simple formulae are presented for calculating the resonant frequencies of a circular sided compact dual-port microstrip antenna. The calculations are in agreement with the experimental observations, with a percentage error of less than two.

Introduction: A dual-port microstrip antenna with a crescent shaped patch with excellent isolation between the ports has been reported [1]. Since circular-sided geometries are more compact than rectangular ones, they find more applications in microstrip arrays. The crescent shaped antenna geometry [1] provides greater area reduction compared to other circular sided patches for broadband operation [2]. In this Letter, formulae for calculating the TM₁₁ and TM₂₁ mode resonant frequencies of this microstrip antenna, obtained by modifying the equations of a standard circular patch [3] are presented. Theoretical results are compared with experimental observations and the validity of the computation is established.

Frequency calculation: The schematic diagram of the antenna is shown in Fig. 1. The antenna geometry is defined by two circular arcs of different radii r_1 and r_2 with their centres c_1 and c_2 displaced by a distance d . The patch is etched on a substrate of thickness h and dielectric constant ϵ_r .

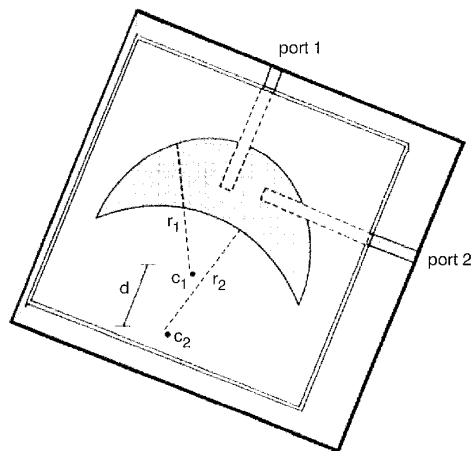


Fig. 1 Geometry of dual-port microstrip antenna

The standard equations for computing the resonant frequencies of a circular patch antenna are modified to take into account the effect of different arc radius and the displacement between the centres of circular arcs in the present geometry.

The TM₁₁, and TM₂₁ resonant frequencies of a circular microstrip antenna of radius r fabricated on a substrate of dielectric constant ϵ_r and thickness h are given by [3]:

$$\text{For TM}_{11} \text{ mode } f_1 = \frac{1.84118c}{2\pi r \epsilon_r \sqrt{\epsilon_r}} \quad (1)$$

$$\text{For TM}_{21} \text{ mode } f_2 = \frac{3.05424c}{2\pi r \epsilon_r \sqrt{\epsilon_r}} \quad (2)$$

$$\text{where } r_c = r \left[1 + \frac{2h}{\pi r \epsilon_r} \left(\ln \frac{\pi r}{2h} + 1.7726 \right) \right]^{1/2} \quad (3)$$

The two resonant frequencies of the crescent shaped patch are calculated as

$$f_{11} = f_1 + df_1 \quad (4)$$

$$f_{21} = f_2 + df_2 \quad (5)$$

When the distance between the centres of the two arcs of the crescent shaped geometry is large, (i.e. $d > 0.04$) the values of f_1 and f_2 are calculated using (1), (2) and (3) with ' r ' replaced by ' r_1 '. If the centres are close, (i.e. $d \leq 0.04$), r is replaced by $r = (3/2)r_1 - (1/2)r_2$ to take into account the effect of r_2 .

The correction terms df_1 and df_2 are calculated as follows:

For $r_2 - r_1 < 0.02$

$$\left. \begin{aligned} df_1 &= \frac{-0.84f_1d}{r_1 + r_2} + \frac{0.17f_1(r_2 - r_1)}{d} \\ df_2 &= \frac{-0.78f_2d}{r_1 + r_2} + \frac{0.23f_2(r_2 - r_1)}{d} \end{aligned} \right\} \text{ for } d < 0.04 \quad (6)$$

$$\left. \begin{aligned} df_1 &= -0.175f_1 - \frac{0.01f_1(r_1 + r_2)}{r_2 - r_1} + \frac{0.019f_1(r_1 + r_2)}{d} \\ df_2 &= -0.17f_2 - \frac{-0.16f_2(r_2 - r_1)}{r_1 + r_2} + \frac{0.01f_2(r_1 + r_2)}{d} \end{aligned} \right\} \text{ for } d \geq 0.04 \quad (7)$$

For $r_2 - r_1 < 0.02$

$$\left. \begin{aligned} df_1 &= \frac{-0.27f_1d}{r_2 - r_1} + \frac{0.082f_1(r_1 + r_2)}{d} - \frac{0.245f_1(r_2 - r_1)}{r_1 + r_2} \\ df_2 &= \frac{-0.275f_2d}{r_2 - r_1} + \frac{0.1f_2(r_1 + r_2)}{d} - \frac{0.22f_2(r_2 - r_1)}{r_1 + r_2} \end{aligned} \right\} \text{ for } d \leq 0.04 \quad (8)$$

$$\left. \begin{aligned} df_1 &= \frac{-0.49f_1d}{r_1 + r_2} + \frac{0.442f_1(r_2 - r_1)}{d} - \frac{0.005f_1(r_1 + r_2)}{r_2 - r_1} \\ df_2 &= \frac{-0.465f_2d}{r_1 + r_2} + \frac{0.48f_2(r_2 - r_1)}{d} \end{aligned} \right\} \text{ for } d > 0.04 \quad (9)$$

Comparison of theory and experiment: The theoretical variation of the two resonant frequencies f_{11} and f_{21} with different values of r_1 , r_2 and d are given in Fig. 2. The experimental results are also plotted in the same Figure for comparison. To further check the validity, the antennas are fabricated on substrates with different dielectric constants and thickness. These results are shown in the Fig. 3. In all these cases the theoretical results are found to be in good agreement with experimental values with an error less than 2%.

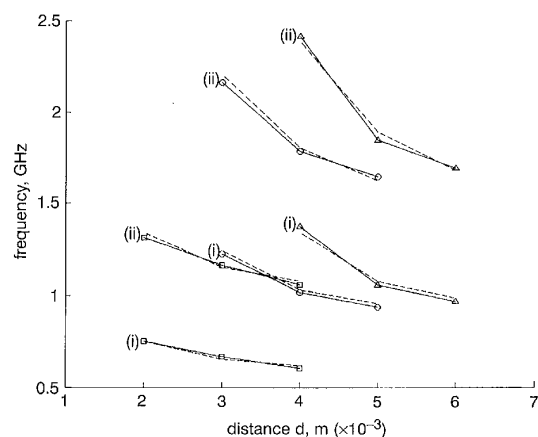


Fig. 2 Variation of TM₁₁ and TM₂₁ mode frequencies with distance between centres of arcs for different r_1 and r_2 ($\epsilon_r = 4.28$, $h = 0.0016$ m)

---- experimental
 --- theoretical
 ○ $r_1 = 0.04$ m, $r_2 = 0.06$ m
 △ $r_1 = 0.04$ m, $r_2 = 0.07$ m
 □ $r_1 = 0.06$ m, $r_2 = 0.07$ m
 (i) f_{11}
 (ii) f_{21}

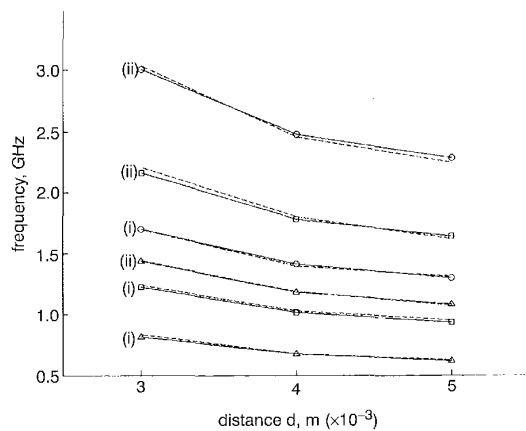


Fig. 3 Variation of TM_{11} and TM_{21} mode frequencies with distance between centres of arcs for different ϵ_r and h ($r_1 = 0.04$ m, $r_2 = 0.06$ m)

--- experimental
 — theoretical
 ○ $\epsilon_r = 2.2$, $h = 0.0008$ m
 △ $\epsilon_r = 10.2$, $h = 0.00066$ m
 □ $\epsilon_r = 4.28$, $h = 0.0016$ m
 (i) f_{11}
 (ii) f_{21}

Conclusion: Empirical formulas to determine the resonance frequencies of the dominant modes of a crescent shaped dual-port microstrip antenna are developed. These calculations are validated by experimental results and the percentage error is found to be less than 2.

Acknowledgments: S.O. Kundukulam (Young collaborator programme) and C.K. Aanandan (Associate scheme) gratefully acknowledge the financial support and facilities provided by the Abdus Salam International Centre for Theoretical Physics (ICTP), Trieste, Italy.

© IEE 2002

11 March 2002

Electronics Letters Online No: 20020956

DOI: 10.1049/el:20020956

S.O. Kundukulam, M. Paulson, C.K. Aanandan, P. Mohanan and K.G. Nair (Centre for Research in Electromagnetics and Antennas, Department of Electronics, Cochin University of Science and Technology, Cochin 682 022, India)

E-mail: aanandan@doe.cusat.edu

References

- KUNDUKULAM, S.O., PAULSON, M., AANANDAN, C.K., and MOHANAN, P.: 'Dual frequency dual polarised crescent-shaped microstrip antenna'. Proceedings of seventh national symposium on Antennas and Propagation, Cochin, 2000, pp. 90–93
- DEHPUKUMAR, M., GEORGE, J., AANANDAN, C.K., MOHANAN, P., and NAIR, K.G.: 'Broadband dual frequency microstrip antenna', *Electron. Lett.*, 1996, **32**, pp. 1531–1532
- BAHL, I.J., and BHARTIA, P.: 'Microstrip antennas' (Artech House, Dedham, MA, 1981)

Detection of microcalcifications in mammograms using local maxima and adaptive wavelet transform analysis

A.M. Bagci and A.E. Cetin

A method for computer-aided diagnosis of microcalcification clusters in mammogram images is presented. Microcalcification clusters which are an early sign of breast cancer appear as isolated bright spots in mammograms. Therefore they correspond to local maxima of the image. The local maxima of the image is first detected and they are ranked according to a higher-order statistical test performed over the subband domain data.

Introduction: Microcalcification clusters are an early sign of breast cancer. The survival rate approaches 100 per cent if cancer is detected early. Microcalcifications (MC) appear as isolated bright spots on mammograms images [1–4].

MCs correspond to local maxima of a mammogram as they are relatively bright and tiny regions in the image. The first step of our method is the detection of the local maxima of the mammogram image. Although a typical mammogram is much smoother than most natural images there are thousands of local maxima in a mammogram image. After detecting the maxima locations we rank them according to a higher-order statistical test performed over the subband domain data obtained by the adaptive wavelet transform. The distribution of wavelet data corresponding to the regular breast tissue is almost Gaussian [3, 4]. However, MCs are different in nature than regular breast tissue and they produce outliers in the subband domain. We take advantage of this fact and rank the local maxima according to a higher-order statistical test estimated in the neighbourhood of each local maximum. When the data is Gaussian the test statistics becomes zero. The higher the value of the test, the higher the rank of the maximum. Peaks due to MCs receive high ranks. The maxima due to small variations in the pixel values and smooth edges became low ranks.

We recently developed methods for detection of MCs based on higher-order statistics, and wavelet analysis [3, 4]. In these schemes the subband (or wavelet) domain image $|x_{hh}| + |x_{hl}| + |x_{lh}|$ of the mammogram image x is divided into overlapping small windows and a higher-order statistic (HOS) [5] is estimated in each window. The windows with HOS values higher than a threshold value T are marked as regions containing MC clusters. A weakness of the methods [3, 4] is that the threshold T should be estimated from a set of training images. The threshold has to be adjusted from scanner to scanner and according to the data set. In addition, we compute the HOS test only around maxima locations instead of the entire image, thus achieving a computationally more efficient method than [3, 4]. The HOS test is reviewed later in this Letter.

Another important feature of this Letter is that an adaptive wavelet (subband) transform [6] is used instead of a regular wavelet transform (WT). It is experimentally observed that adaptive WT provides better results than the ordinary Daubechies WT.

Adaptive wavelet transform: Classical adaptive prediction concepts are combined with the perfect reconstruction filter bank theory in [6] where the key idea is to decorrelate the polyphase components of the multichannel structure using an adaptive predictor P as shown in Fig. 1. Adaptation of the predictor coefficients are carried out by a least mean square (LMS)-type algorithm.

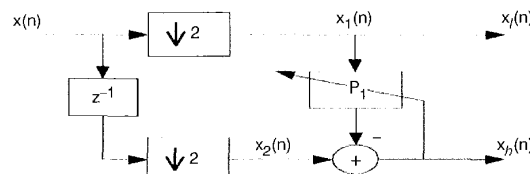


Fig. 1 Analysis stage of two-channel adaptive filter bank structure (P_1 represents an adaptive predictor)

In Fig. 1, $x_1(n)$ is the downsampled version of the original signal, $x(n)$, thus it consists of the even samples of $x(n)$. Similarly, the signal $x_2(n)$ consists of the odd samples. An LMS-based FIR predictor of $x_2(n)$ from $x_1(n)$ can be expressed as $\hat{x}_2(n) = \mathbf{w}(n)\mathbf{x}_1^T(n)$ where $\mathbf{x}_1(n) = [x_1(n-L), \dots, x_1(n+L)]^T$ is the observation vector, and the $2L+1$ vector $\mathbf{w}(n)$ is the vector of predictor coefficients which is adapted by the equation

$$\mathbf{w}(n+1) = \mathbf{w}(n) + \mu \frac{\mathbf{x}_1(n)e(n)}{\|\mathbf{x}_1(n)\|^2} \quad (1)$$

where the error signal $e(n) = x_2(n) - \hat{x}_2(n)$.

The filterbank structure shown in Fig. 1 is the simplest adaptive wavelet transform (AWT) structure. In this structure, the 'highband signal' is essentially the prediction error and as a result the subsignals are expected to be decorrelated. Other AWT structures with antialiasing filters for the upper branch signal can be found in [6].